Spontaneous thermoreversible formation of cationic vesicles in a protic ionic liquid (Supporting Information)

Carlos R. López-Barrón,[†,‡] Dongcui Li,[†] Leo DeRita,[†] Madivala G. Basavaraj,[†,¶] and Norman J. Wagner[*,†]

Center for Neutron Science, Department of Chemical and Biomolecular Engineering, University of Delaware, Newark, DE 19716, USA

E-mail: wagnernj@udel.edu

Experimental Procedure

Materials. Didodecyldimethylammonium bromide (DDAB, Tokio Tsei, 98 %) was recrystallized first from a mixture of acetone (Fisher, 99.7%) and ethyl ether (Fisher, 99.5%) and then from ethyl acetate (Fisher, 99.9%), following procedures previously reported.[1,2] In short, a saturated DDAB solution (5 g of DDAB in 60 ml in an eqivolume acetone/ethyl ether mixture) was heated to 30 °C and filtered through a Böchner funnel with Whatman filter paper (No.1) to remove any insoluble impurities. The filtered solution was cooled down to 4 °C and the crystallized DDAB was collected. Subsequently DDAB crystals were dissolved in 60 ml of ethyl acetate to make a

[*]To whom correspondence should be addressed

[†]Center for Neutron Science, Department of Chemical and Biomolecular Engineering, University of Delaware, Newark, DE 19716, USA

[‡]Current address: ExxonMobil Chemical Company, Baytown, Texas, 77520, USA

[¶]Current address: Department of Chemical Engineering, Indian Institute of Technology, Madras Chennai 600 036, India

saturated solution and heated to 40 °C. The warm solution was filtered and DDAB recrystallized by cooling down to 4 °C. the DDAB crystals were collected and washed with ether and finally were dried in a vacuum oven at 60 °C for 30 minutes. Complete solvent removal was confirmed by gravimetry. The purity of the recrystallized DDAB was verified by ^{1}H NMR and ^{13}C NMR measurements. Figure S1 shows the proton NMR spectra for the unpurified and the purified DDAB, as well as that reproduced from SciFinder (Chemical abstracts Service), as a reference. The ^{1}H NMR spectra of the unpurified DDAB shows a small peak that disappear after recrystallization. No differences between the ^{13}C NMR spectra of unpurified and recrystallized DDAB (Figure S2) were observed. It is worth mentioning that the small amount of impurities detected by proton NMR had no influence on the phase behavior of DDAB solutions.

Ethylammonium nitrate (EAN, Iolitec, 99 %) was deuterated by mixing with equimolar amounts of D_2O, and subsequent heating to 40 °C for three hours. Immediately afterwards, the mixture was heated to 90 °C under vacuum for 24 hours to remove the water, after which it was remixed with fresh D_2O. This cycle was repeated three times, resulting in substitution of about 86 % of the amino-hydrogens with deuterium, as confirmed by ^{1}H NMR. Figure S3 shows the spectra obtained for pure EAN before and after deuteration, as well as their peak assignments. The level of deuterium substitution is obtained from the difference in the areas under the H_1 peak, which are indicated under the spectra. The water content, after the last drying cycle, was 0.13 wt% (measured by Karl Fischer titration).

Phase behavior. DDAB/EAN solutions with concentration ranging from 1 wt% to 95 wt% were prepared in capped vials. The samples were homogenized by immersing the vials in an oil bath set to 80 °C for at least 24 hrs. The phase behavior of DDAB/EAN solutions was studied by visual inspection of the samples immersed in an oil bath with controlled temperature. After setting the desired temperature, samples were left to equilibrate for 24 hours. The temperature range tested was 15 $°C < T <$ 120 $°C$ with steps of 5 °C; except for the temperatures around 35 °C, for which the steps were in increments of 1 °C. The sample compositions range studied here is 1 wt% $\leq$ [DDAB] $\leq$ 75 wt%, with steps of 5 wt%, except for compositions near the phase limits

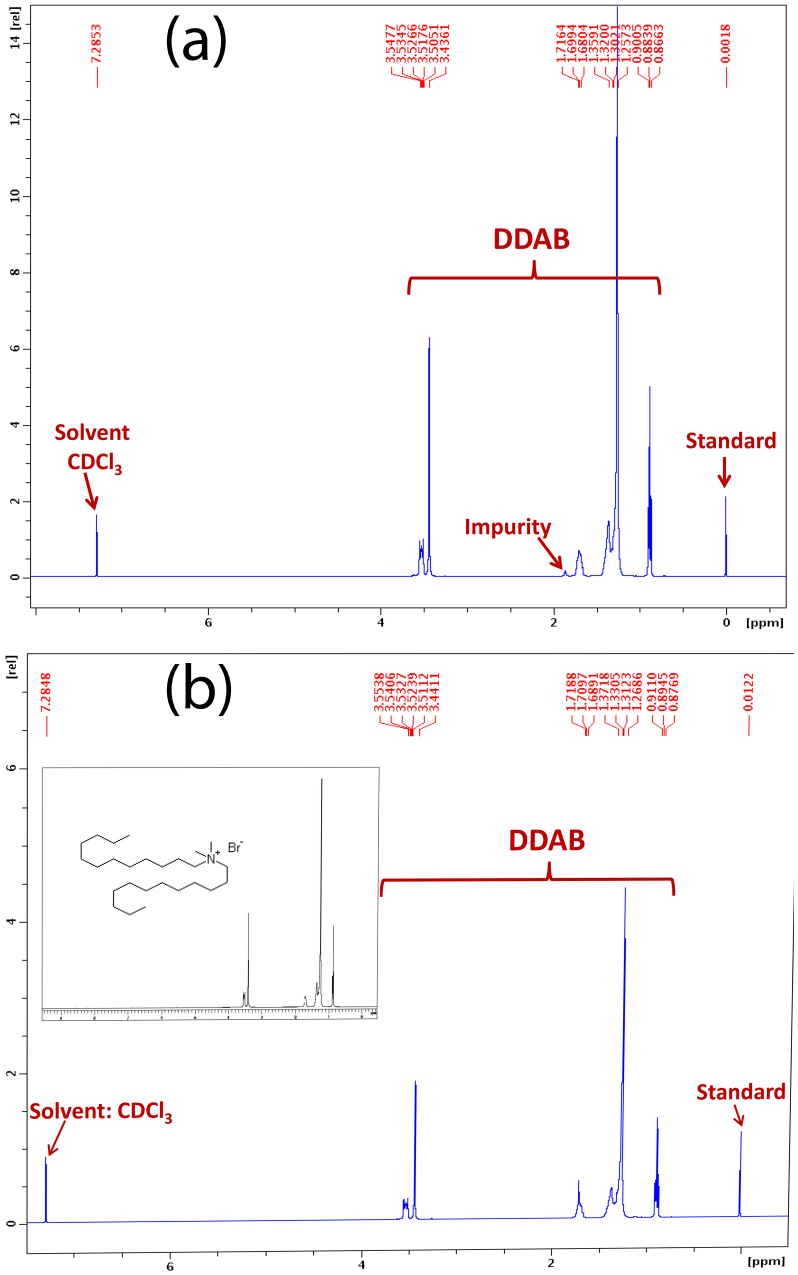

Figure S1. ^{1}H NMR spectra for DDAB in $CDCl_3$ at 25 °C (a) before and (b) after recrystallization. The inset in (b) shows the spectra taken from SciFinder; Chemical Abstracts Service: Columbus, OH; proton NMR spectrum, spectrum ID WHSP45017; https://scifinder.cas.org (accessed July 13, 2012).

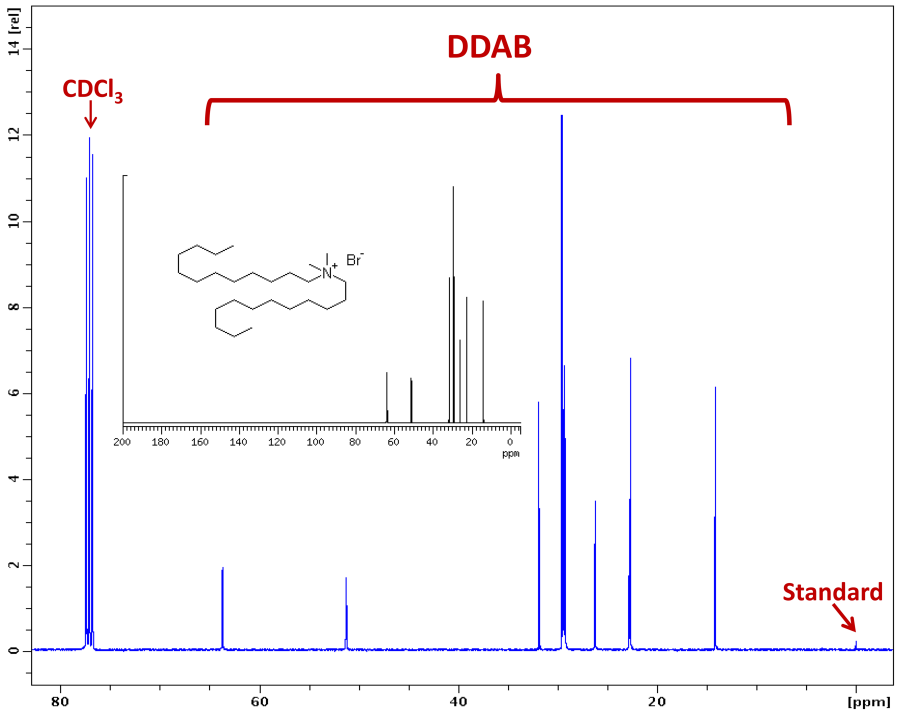

Figure S2. ^{13}C NMR spectra for recrystallized DDAB $CDCl_3$ at 25 °C. The inset shows the spectra taken from SciFinder; Chemical Abstracts Service: Columbus, OH; carbon-13 NMR spectrum, spectrum ID WCDS11418; https://scifinder.cas.org (accessed July 13, 2012).

(1.9 wt% and 68 wt%), for which the steps where of 0.1 wt%. Figure S4 shows pictures of vials containing DDAB/EAN solutions with different compositions, within the two-phase region, along with the volume fraction of the lower phase (calculated as the height ratio: h/H) as a function of DDAB wt%. Notice that the volume fraction line lies below the straight (dashed) line calculated with the lever rule (LP mass fraction $(\text{lever rule}) = [68 - \text{DDAB wt\%}]/[68 - 1.9]$). This negative excess volume of mixture indicates a decrease of the partial molar volume of both DDAB and EAN when mixed as compared to their molar volume when pure.

Bright field microscopy (BFM). BFM was carried out using an (IX2 Olympus) inverted microscope with 10X and 20X objectives. A drop of each sample was put in between two glass cover slip separated by glass spacers (thickness $\sim$ 0.5 mm) and sealed with UV-curing adhesive. The cover slips were put on an home-made aluminium plate whose temperature is controlled by circulating water (from a Julabo refrigerator/heating circulator bath) through inner channels. Micrographs of the samples were taken at temperatures ranging from 15 °C to 80 °C. The temperature

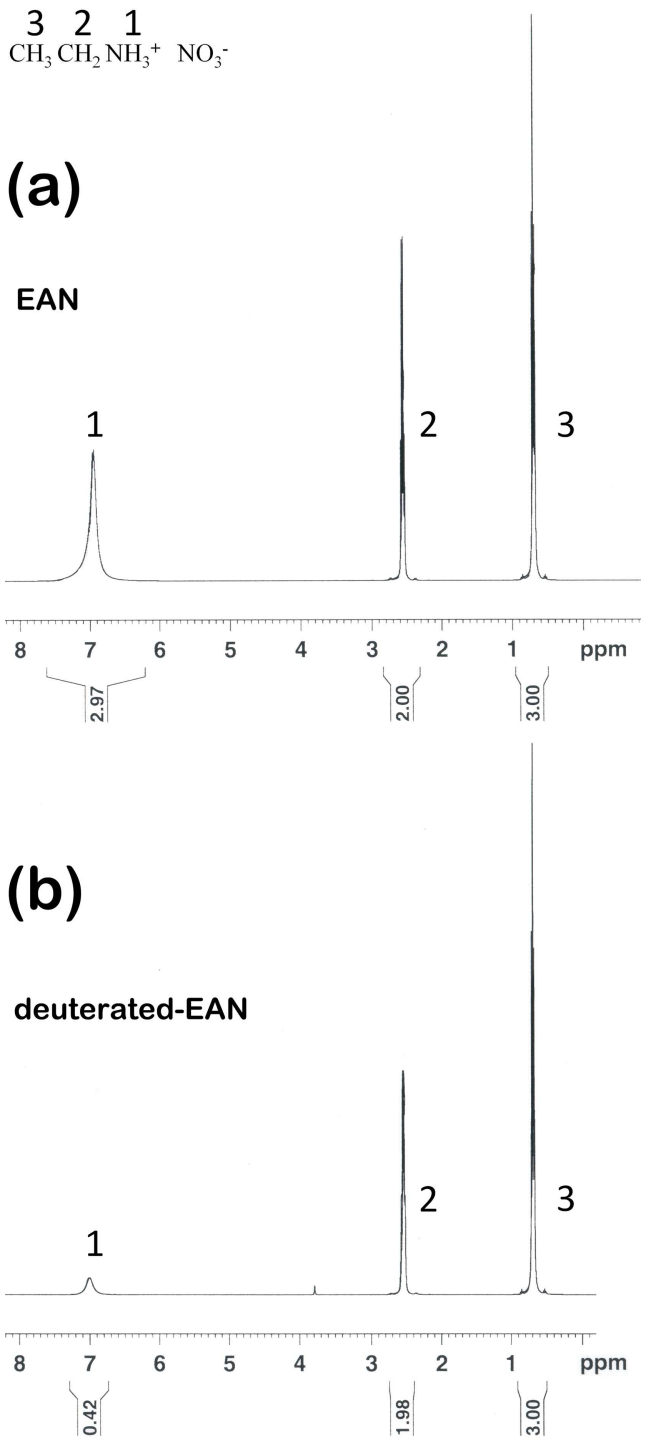

Figure S3. ^{1}H NMR spectra for pure EAN at 25 °C (a) before and (b) after deuteration.

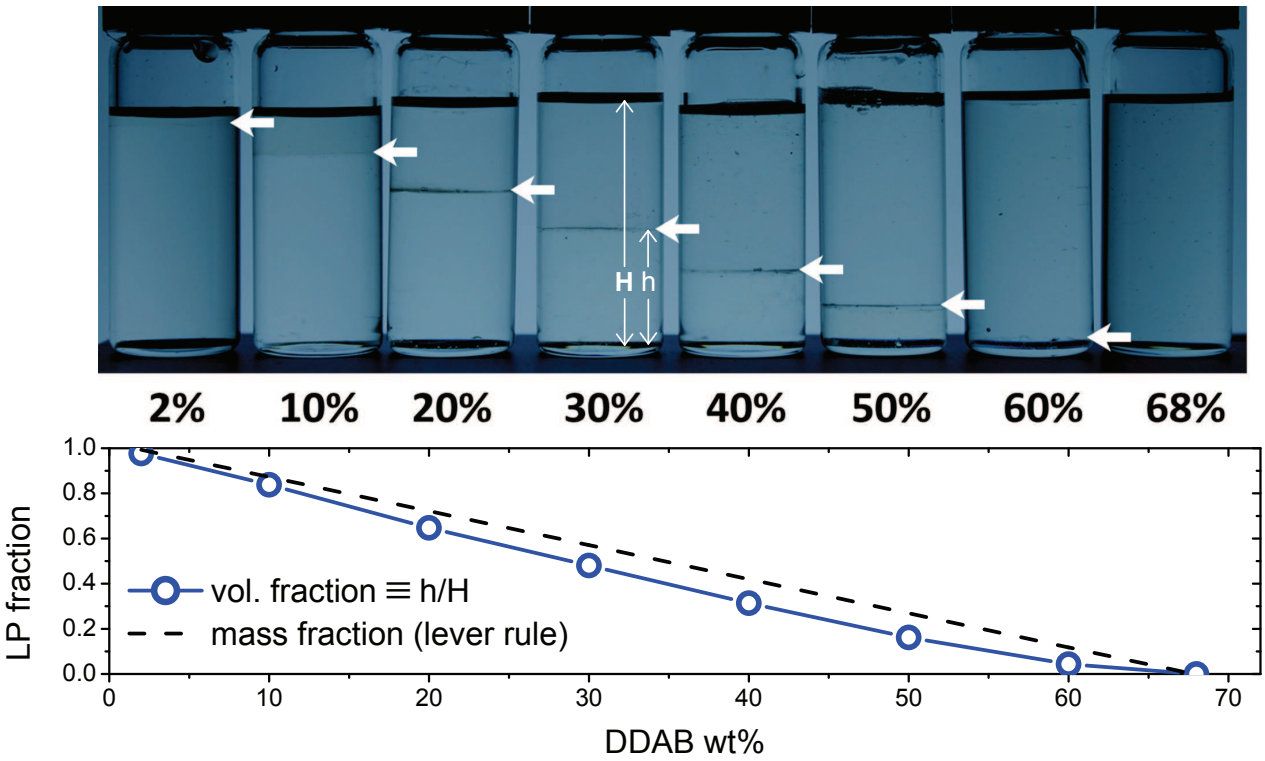

Figure S4. Upper panel: DDAB/EAN solutions with the indicated compositions. White arrows indicate the position of the lower phase (LP)/uper phase(UP) interface. The total height of the solutions and the height of the LP are indicated by the symbols: H and h, respectively. Lower panel: Volume and mass fractions of the LP correspnding to the solutions shown in the upper panel. The volume fraction is calculated as h/H, whereas the mass fraction is calculated using the lever rule.

was measured by immersing a thermocouple directly into the sample.

Figures S5 and S6 show representative micrographs of samples from extracted lower phase (LP) and upper phase (UP) of biphasic DDAB/EAN solutions under equilibrium conditions (2 hrs of equilibration) at 25 °C (after loading), 65 °C and 25 °C (after cooling from 65 C). In general, vesicles are observed after loading the samples but with higher polydispersity than those formed after cooling from 65 °C. This could be due to mechanical mixing during pippeting (loading). Vesicles dissapear after heating above 35 °C. The absence of vesicles was verified by keeping some samples for longer time (> 72 hrs) at 65 °C. Additionally, several heating-cooling cycles were repeated and similar behavior of vesicle disappearance-reformation was observed. It is found that the sample after one heating-cooling cycle shows less polydispersity than that without subjecting to any heating-cooling cycles.

Rheology. Rheological characterization was performed on a strain-controlled rheometer (ARES G2, TA Instruments) with cone and plate geometry. Dynamic temperature ramps (with strain of 0.2, ω = 1 rad/s) where carried out with heating/cooling rate of 1 °C/min and temperature range: 15 $°C \leq T \leq$ 80 °C). Regardless the composition and the temperature, all the samples in the composition range reported here showed Newtonian behavior, i.e., they showed negligible elastic modulus and shear rate independent viscosity.

Small and ultra-small angle neutron scattering (SANS and USANS). SANS and USANS were carried out at the National Institute of Standards and Technology (NIST) Center for Neutron Research (NCNR) on the NG-7 30 m instrument (using neutrons with mean wavelength $\lambda = 6$ Å and wavelength spread (FWHM) of $\Delta\lambda/\lambda = 11\%$) and on the perfect crystal difractometer (with mean $\lambda = 2.4$ Å),[3] respectively. Sample to detector distances of 1 m (with 25 cm offset), 4 m, and 15.3 m were used for SANS measurements to cover a $q-$range of 0.008 to 7.0 nm^{-1}. Samples were held in standard (1 mm) titanium cells with quartz windows. The cell temperature was equilibrated for 30 min before the measurements using a Julabo temperature bath unit. SANS and USANS data were reduced and analyzed using IGOR Pro macros available from NIST.[4] Circular averaging was used to compute the average absolute, angle-independent scatter intensity, $I(q)$.

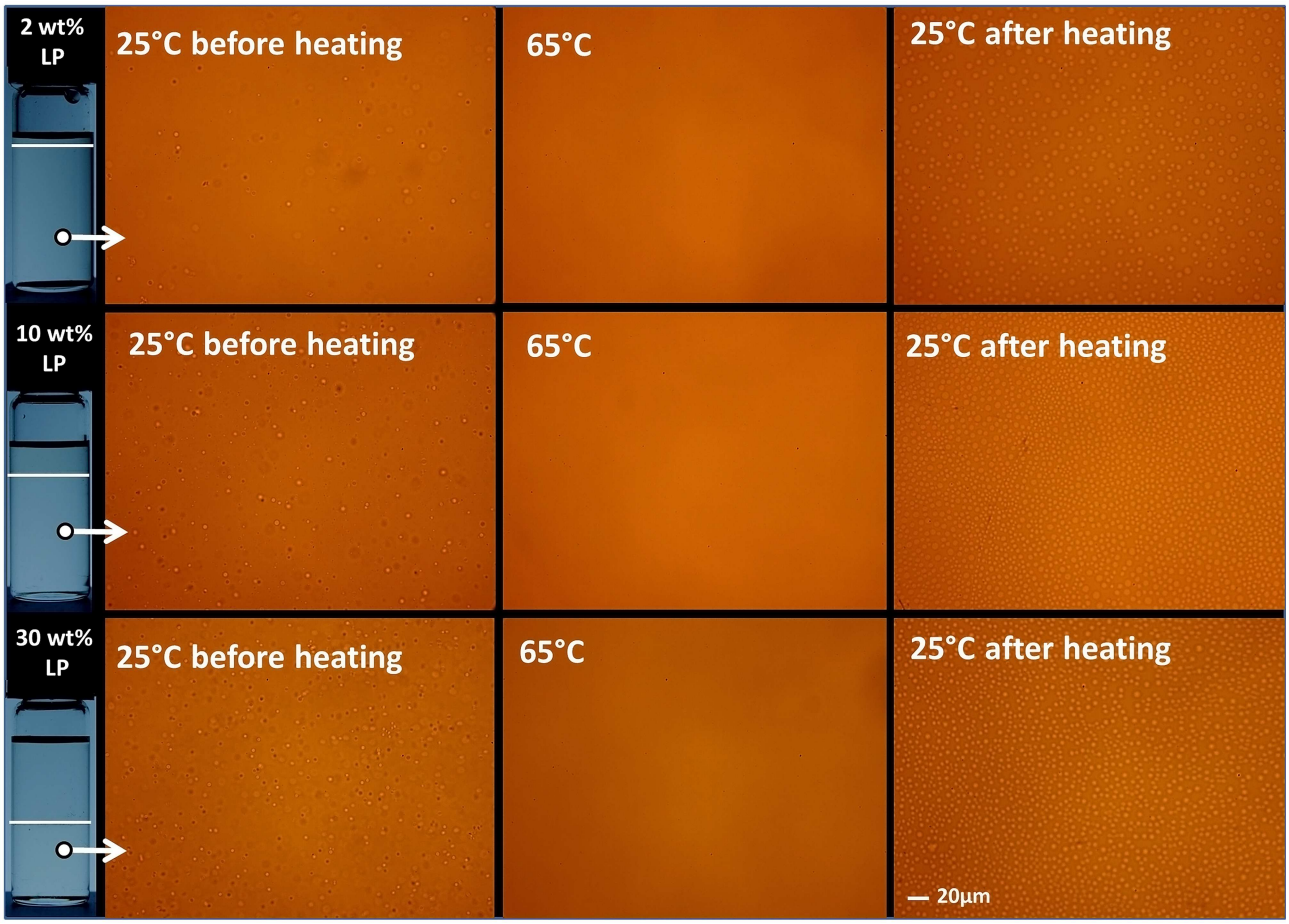

Figure S5. BFM micrographs of the lower phase of 2 wt% (upper row), 10 wt% (middel row) and 30 wt% (lower row) DDAB/EAN solutions. Micrographs taken after loading the samples at 25 °C and two hours of equilibration (left column), after heating to 65 °C (middle column) and after cooling from 65 °C to 25 °C (right column). The scale bar is common for all nine micrographs. The horizontal white lines in the vial pictures (left) mark the position of the LP/UP interface.

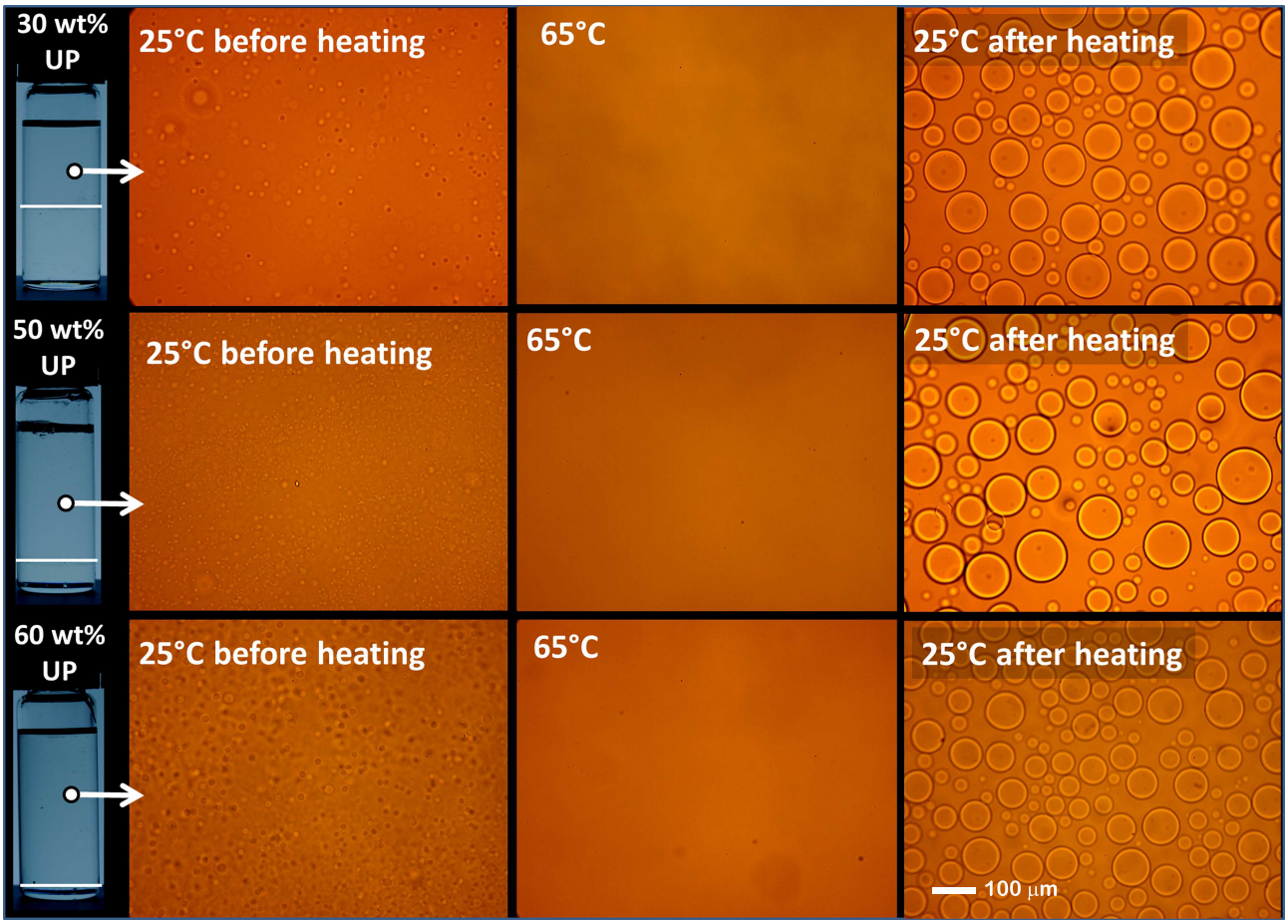

Figure S6. BFM micrographs of the upper phase of 30 wt% (upper row), 50 wt% (middel row) and 60 wt% (lower row) DDAB/EAN solutions. Micrographs taken just after loading at 25 °C (left column), after heating to 65 °C (middle column) and after cooling from 65 °C to 25 °C (right column). The scale bar is common for all nine micrographs. The horizontal white lines in the vial pictures (left) mark the position of the LP/UP interface.

Proving Equilibrium State of the Vesicular Phase

Probability density (for vesicle diameter). The core diameter, D_c, of more than 1500 vesicles in each sample were measured from the BFM micrographs and the diameter density distribution calculated, using ImageJ (http://imagej.nih.gov/ij/). The probability density function is defined as

$$P_D(D_c) = \frac{\pi n_i \left(\frac{D_{c,i}}{2}\right)^2}{A_T} \tag{S1}$$

where $D_{c,i}$ and n_i are the vesicle diameter of the $i-$th bin center and its frequency count, respectively. A_T is the total area of the micrograph. P_D was defined in such a way that $\sum_{i=1}^{N} P_D = A_A$, where N in the total number of bins and A_A is the area fraction. The volume fraction, Φ, is readily obtained with the stereological relation: $A_A = \Phi$.[5]

Three key experiments were performed to verify that the vesicular phase, LV, exists in a state of true thermodynamic equilibrium:

(1) Cooling of a 1.8 wt% solution from 65 °C to 25 °C. The sample was loaded to the aluminium plate at room temperature and then heated and equilibrated at 65 °C. Subsequently, the plate was cooled to 25 °C and micrographs were taken every 5 minutes during the cooling process. As discussed in the paper, no vesicles are observed at 65 °C, whereas at room temperature they form spontaneously.

(2) Heating of a 1.8 wt% solution from 2 °C to 25 °C. The sample was put in the refrigerator (at 2 °C) overnight to reach equilibrium. The microscope stage was pre-cooled at 2 °C via an ice-water bath for at least 2 hrs before loading the sample. The stage temperature was well kept at 2 °C via reading the thermocouple on the stage. The sample was quickly transferred to the stage and was equilibrating for at least 4 hrs after loading. Note that the reported melting temperature of EAN is 14 °C, however, the solution remained fluid at the refrigerator temperature (at 2 °C). This could indicate a depression in the melting temperature due to the presence of the surfactant; however, the proof of this hypothesis is beyond the scope of this study. Interesting, no vesicles were observed at the refrigerator temperature (2 °C), as shown in Figure S7. After equilibration at

2 °C on the microscope stage, the water bath temperature was set to 25 C. Micrographs were taken every 5 minutes to monitor the vesicle formation. Vesicle slowly form as the temperature reached 25 °C (Figure S7).Ť

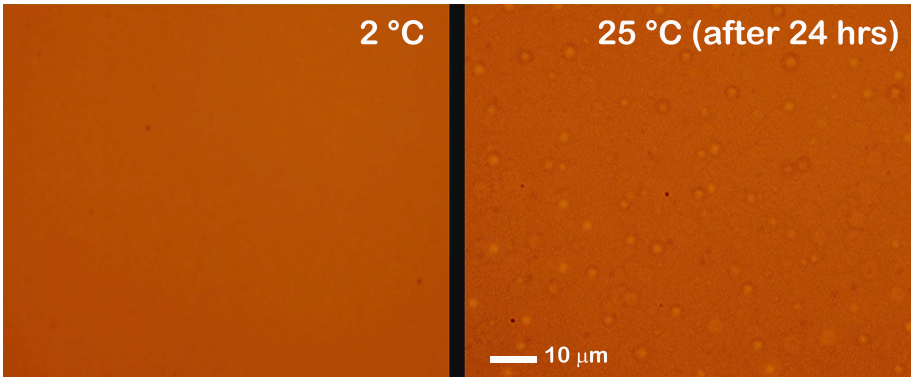

Figure S7. BFM micrographs of 1.8 wt% DDAB/EAN solution at (left) 2 °C and right 25 °C, after heating from 2 °C and equilibrating for 24 hours.

(3) Dissolution from a concentration of 70 wt% to 1.8 wt%. A 70 wt% sample in the microscope stage (at 25 °C). Subsequently, enough EAN to reduce the composition to 1.8 wt% was added to the sample in the glass slide and micrographs were taken at 5 min intervals. The dissolution and equilibration processes occurred slowly and in several stages (see Figure S8). As soon as pure EAN is added to the concentrated solution, small droplets of the latter were observed floating on a lower phase, which indicates that dissolution is not instantaneous. After 24 hrs, giant vesicles (GVs) form inside the droplets. At later times (48 hrs), large vesicles (LVs) start to form and the droplets of concentrated solutions (with the GVs inside) start to decrease in size. Eventually, the droplets disappear completely and only LVs are observed. The same sequence of events (except for the last droplet disappearance) is shown in a movie (included in the Supporting Information) of a 2 wt% solution upon cooling. Notice that the 2 wt% solution is a biphasic sample, hence the equilibrium state shows small droplets of the upper phase, containing giant vesicles, floating on the lower phase, containing large vesicles (see the movie named “Spontaneous formation of large and giant vesicles.qt” in the Supporting Information).

Figure S9 shows the vesicle diameter distribution of (a) LP of 30 wt% solution at 25 °C after cooling from 65 °C, (b) 1.8 wt% solution at 25 °C after cooling from 65 °C, (c) 1.8 wt% solution

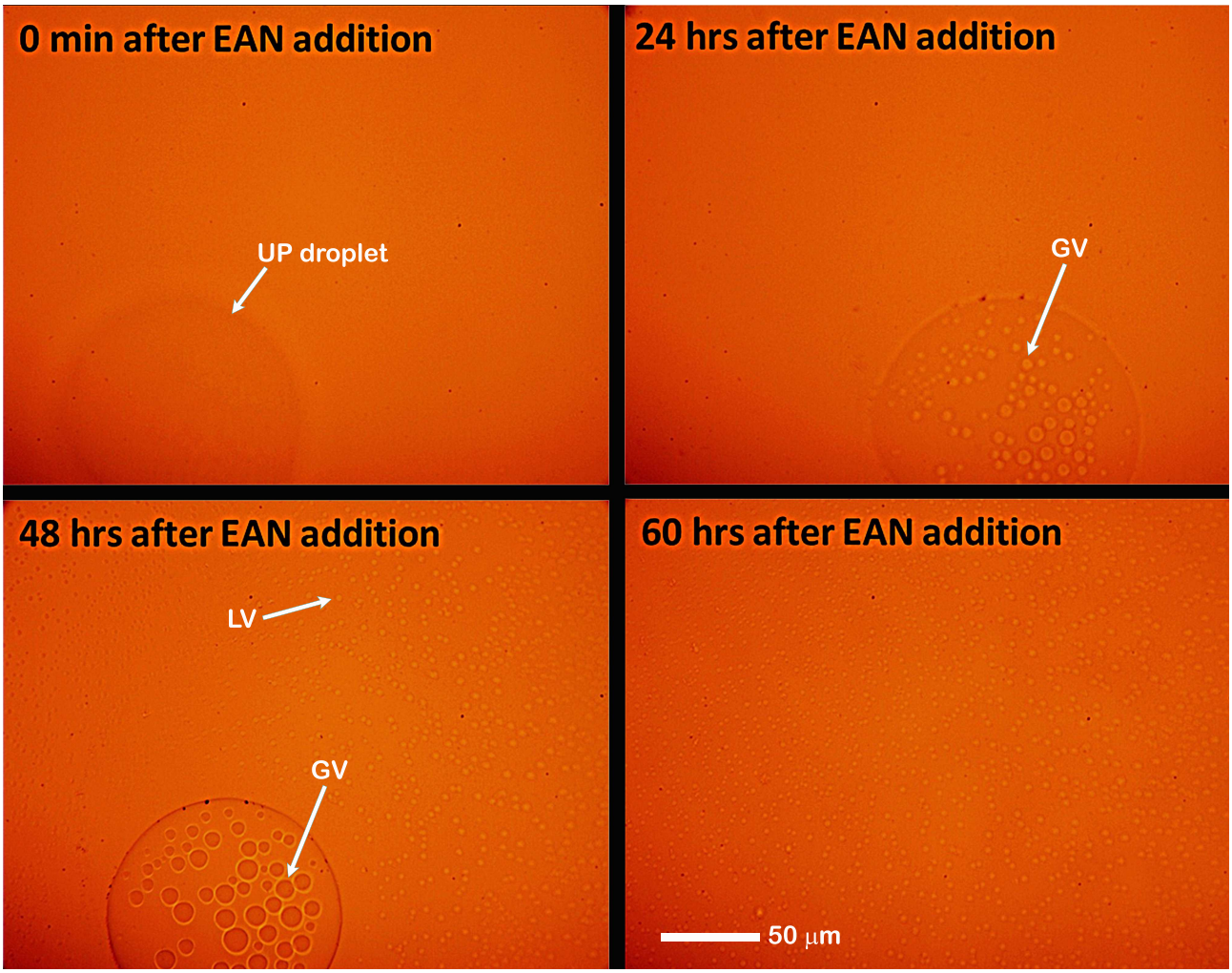

Figure S8. BFM micrographs of 1.8 wt% EAN/DDAB solution after dilution from a 70 wt% solution. Micrographs were taken at the indicated times, after the EAN addition to the concentrated solution.

at 25 °C after heating from 2 °C, and (d) 1.8 wt% at 25 °C after 60 hrs of dissolution from a 70 wt% solution. Clearly, the four distributions are very similar, with an overall average diameter and polydispersity (defined as $PDI = 2\sigma/\bar{D}_c$, where σ^2 is the variance of the distribution) of 2.89 ± 0.4 μm and 0.24 ± 0.03, respectively. The path independence for vesicle formation strongly supports that vesicles exist in a true thermodynamic equilibrium.

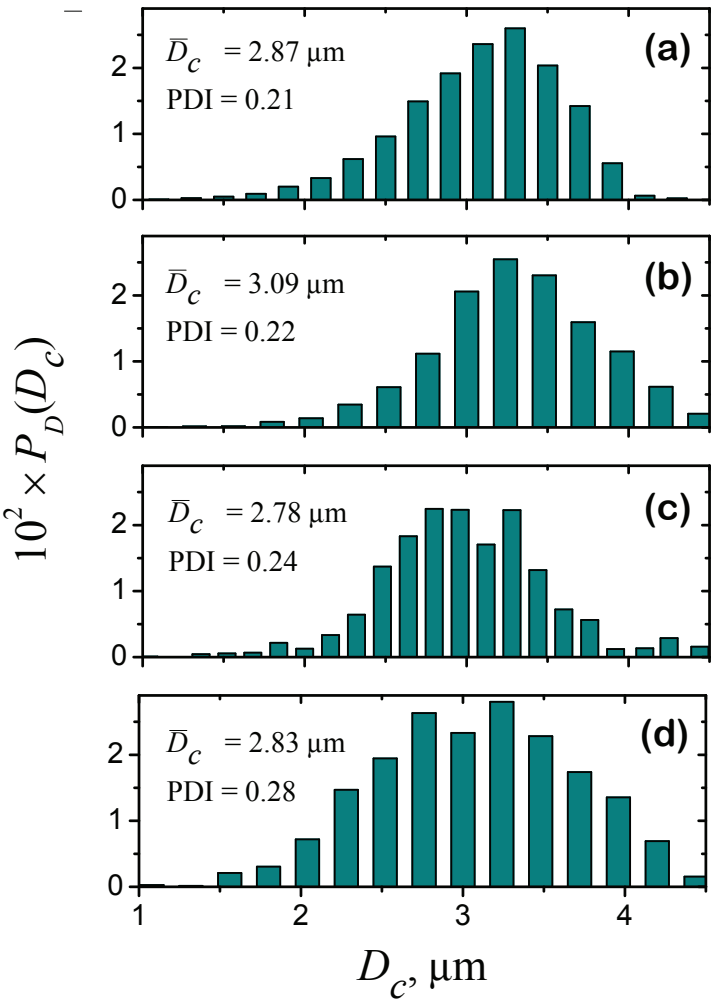

Figure S9. Vesicle diameter distribution(measured at 25 °C) for (a) the lower phase of 30 wt% DDAB/EAN solution, (b) 1,8 wt%, after cooling from 65 °C, (c) 1.8 wt%, after heating from 2 °C, and (d) 1.8 wt%, after dilution from a 70 wt% solution.

Mass Balance of the Biphasic Solutions

Here, we confirm the consistency of the methods used for structure determination (i.e., BFM and SANS) by checking the mass balance for the phase splits observed in the DDAB/EAN solutions. SANS is an absolute method and can be used to determine mesophase composition. The bilayer thickness is obtained from SANS and the vesicle diameter distributions are measured with BFM. BFM measures a 2-dimmensional image and the phase composition is characterized as area fraction, A_A [§]. For the samples DE2 and DE30LP, the global volume fraction of surfactant in the vesicle shell (Φ_s), core (Φ_c) and medium (Φ_m) are computed with

$$\begin{aligned} \Phi_s &= A_{A,s} \\ \Phi_c &= \phi_c A_{A,c} \\ \Phi_m &= \phi_m A_{A,m} \end{aligned} \tag{S2}$$

where ϕ_c and ϕ_m (presented in Table 1) are the individual phase volume fractions of the core and medium, respectively, measured by SANS. $A_{A,s}$, $A_{A,c}$ and $A_{A,m}$ are the area fractions of the shell, core and medium, respectively, measured directly from the BFM as

$$\begin{aligned} A_{A,s} &= \frac{\pi}{A_T} \sum_{i=1}^{N} \left(\frac{D_{c,i}}{2} + \delta\right)^2 - \left(\frac{D_{c,i}}{2}\right)^2 \\ A_{A,c} &= \frac{\pi}{A_T} \sum_{i=1}^{N} \left(\frac{D_{c,i}}{2}\right)^2 \\ A_{A,m} &= 1 - A_{A,s} - A_{A,c} \end{aligned} \tag{S3}$$

where $D_{c,i}$ is the diameter of the i-th vesicle, N is the total number of vesicles measured in a total area A_T.

The bilayer (shell) thickness, δ, is obtained with $\delta = \Phi_{L_3} d$ (see inset in Figure 4), where Φ_{L_3} is the volume fraction of the bilayer in the L_3 phase and d is the d-spacing obtained by fitting the

[§]We use nomenclature used in stereology textbooks[5] for the geometrical parameters

SANS data with the Teubner-Strey (TS) model. The volume fraction can be obtained with

$$\Phi_{L_3} = \frac{w}{w + (1-w)\frac{\rho_{DDAB}}{\rho_{EAN}}} \tag{S4}$$

where w is the measured weight fraction. ρ_{DDAB} and ρ_{EAN} are the DDAB and EAN (mass) densities, respectively, which, at 25 °C, are $\rho_{DDAB} = 0.941$ g/ml and $\rho_{EAN} = 1.236$ g/ml (measured with a density meter DMA 45000M, Anton Paar). Hence, for $w = 0.68$ (solution DE68), $\Phi_{L_3} = 0.737$. The DE68 SANS data fitted with the TS model gives $d = 2.95$ nm. Therefore, $\delta = \Phi_{L_3} d = 2.09$ nm. This value is consistent with that reported by Dubois and Zemb for DDAB in water ($\delta_{DDAB/H_2O} = 2.4$ nm).[6] For the DE30UP sample, SANS data fitting gives $d = 2.98$ nm, hence the volume fraction, $\Phi_{L_3} = \delta/d = 0.702$.

The volume fraction of the surfactant in the shell of the giant vesicles is in the order of 1×10^{-4}, hence it is neglected in this calculation. The total volume fraction for the 30 wt% DDAB/EAN solution is calculated with

$$\Phi_T = (\Phi_s + \Phi_c + \Phi_m)\,\varphi_{LP} + \Phi_{L_3}\varphi_{UP} \tag{S5}$$

where φ_{LP}(=0.42) and φ_{UP}(=0.58) are the macroscopic volume fractions of the lower and upper phases, respectively.

Table S1 show the calculated volume fractions and the estimated weight fractions. It should be noted that the volume fraction of DE30LP (given by $\Phi_s + \Phi_c + \Phi_m$) is very similar to that of the sample DE2, and similarly, the volume fraction of DE30UP is close to the corresponding value for DE68. This indicates that the phase separation leads to coexisting phases with compositions close to the boundaries of the two phase region in the DDAB/EAN phase diagram (Figure 1). As the tie lines must be horizontal (i.e., isothermal), this calculation confirms that the phase split is between the soluble-monomers and L_3 phases.

Table S1. Volume fractions and weight fractions for the DDAB/EAN solutions.

Sample	$w_{meassured}$	Φ_s	Φ_c	Φ_m	$^a\Phi_{LV}$	Φ_{L_3}	Φ_T	$w_{estimated}$
DE2	0.019	9.5E-4	8.30E-3	1.12E-2	2.04E-2	– –	2.04E-2	0.016
DE30LP	^{b}0.30	1.2E-3	1.04E-2	1.05E-2	2.18E-2	– –	0.418	0.34
DE30UP		– –	– –	– –	– –	0.702		
DE68	68	– –	– –	– –	– –	0.743	0.743	0.68

$^a\Phi_{LV} = \Phi_s + \Phi_c + \Phi_m$

^{b}Global weight fraction, i.e., considering both lower and upper phases.

Structural Analysis of the Giant Vesicles and the L_3 Phase.

As discussed in the paper, structural details of the giant vesicles are not detected by neutron scattering techniques (SANS and USANS). However the vesicle diameter is readily measured by BFM. The mean diameter (D_c), and polydispersity (PDI) of the giant vesicles in the upper phase of the 30 wt% and in the 68 wt% solutions are shown in Table S2.

For the L_3 phase, whose scattering peak was fitted to the Teubner-Strey (TS) model (Eqn. 2 in the paper),[7] two characteristic length scales can be obtained from the parameters a_2, c_1 and c_3: a domain periodicity,

$$d = 2\pi \left(\frac{1}{2} \left(\frac{a_2}{c_2} \right)^{1/2} - \frac{1}{4} \frac{c_1}{c_2} \right)^{-1/2} \tag{S6}$$

and a correlation length scale,

$$\xi = \left(\frac{1}{2} \left(\frac{a_2}{c_2} \right)^{1/2} + \frac{1}{4} \frac{c_1}{c_2} \right)^{-1/2} \tag{S6}$$

which reflects the short-range order among the domains. The computed d and ξ values for the samples DE30UP and DE68 are shown in Table S2. Also shown in Table S2 are the average thickness of the EAN channels in the L_3 phase ($d_{EAN} = d - \delta$) and the volume fraction ($\Phi_{L_3} = \delta/d$).

Table S2. Parameters from BFM analysis and from SANS modeling for DE30UP and DE68 at 25 °C and 80 °C.

Sample	T (°C)	BFM D_c (μm)	BFM PDI	SANS ξ (nm)	SANS d (nm)	SANS δ_{EAN} (nm)	SANS δ/d
DE30UP	25	26.5	0.31	2.51	2.98	0.88	0.70
	80	– –	– –	2.27	2.92	0.82	0.72
DE68	25	32.6	0.30	2.37	2.95	0.85	0.71
	80	– –	– –	2.09	2.88	0.78	0.73

Viscosity-structure relationship for the L_3 phase.

Figure S10 shows the temperature dependence of viscosities for the four samples studied here. The viscosity of all the samples is shear-rate independent (i.e., all the samples are Newtonian) throughout the temperature range investigated. The viscosities of DE30LP, DE2 and EAN are essentially the same at all temperatures. In contrast, DE30UP and DE68 display viscosities of at least one order of magnitude larger than EAN and exhibit a different temperature dependence. This shows that the viscosity is sensitive to the bilayer microstructure.

The viscosity of EAN measured here is in agreement to that reported by Weingärtner and coworkers[8] (also shown in Figure S10). They fit the data to an Arrhenius expresion

$$\eta = \eta_\infty e^{E_a/RT} \tag{S8}$$

in the range $15°C \leq T \leq 45°C$ (dashed line in Figure S10), obtaining an activation energy $E_a = 24.5 kJ/mol$. However, Eq. S8 does not fit the viscosity data in the whole temperature range studied here. To account for this, we used the empirical Vogel-Tammann-Fulcher (VTF) equation[9–11]

$$\eta = A e^{B/(T-T_0)} \tag{S9}$$

where A and B are fitting parameters and T_0 is the Vogel temperature. Equation S9 is normally used to describe the temperature dependence of the viscosity (and conductivity) of ionic liquids.[12–21]

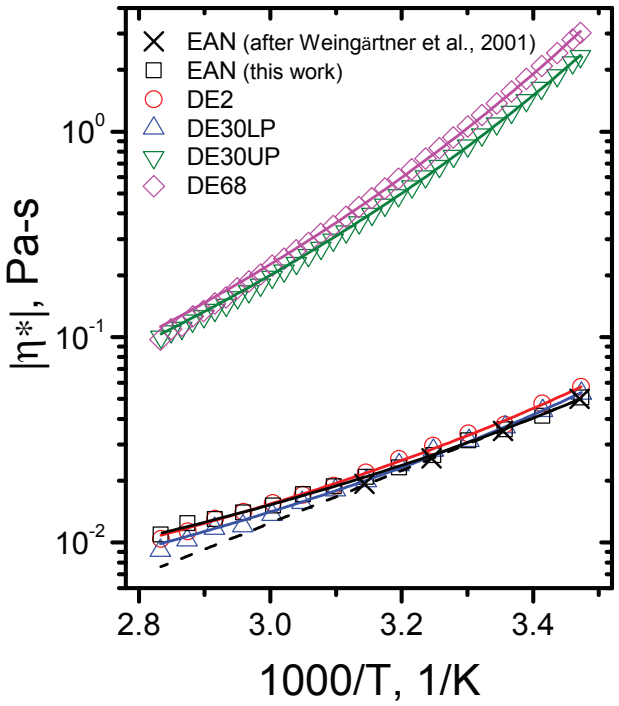

Figure S10. Temperature dependence of the complex viscosity for EAN and DDAB/EAN solutions. Solid (curved) lines are fits to VTF equation (Eq. S10) with the parameters shown in Table S3. Crosses are data for EAN reported by Weingärtner and coworkers[8] and the dashed (straight) line is the fit of these data to Arrhenius equation.

The VTF equation accounts for the extraordinary slowing down of the relaxation and transport (viscosity and diffusion) mechanisms occurring as the system approaches the glass transition temperature (T_g).[22] Hence, T_g is commonly used as the Vogel temperature.[12,16,18,20,23] The VTF parameter $B = E_a/R$,[12] such that Eq. S9 becomes

$$\eta = Ae^{E_a/R(T-T_g)} \tag{S10}$$

The solid lines in Figure S10 are fits for the viscosity data using the modified VTF equation (Eq. S10). The VTF parameters are shown in Table S3. We use the T_g value for EAN previously measured calorimetrically ($T_{g,EAN} = -182$ K[24]). The activation energy for the dilute solutions is slightly higher with respect to EAN, whereas for the concentrated solutions it is about two times higher. This reflects the restriction to flow imposed by the bilayer bicontinuous structure. In a separate paper, we show that VTF equation also describes the temperature dependence of the viscosity and conductivity of concentrated DDAB/EAN solutions.[25]

Table S3. VTF fitted parameters for EAN and DDAB/EAN solutions.

Sample	A, Pa-s	E_a, kJ/mol	T_g, K
EAN	9.49×10^{-4}	3.49	182
DE2	7.59×10^{-4}	3.84	182
DE30LP	6.24×10^{-4}	3.91	182
DE30UP	6.23×10^{-4}	7.25	182
DE68	5.63×10^{-4}	7.44	182

Finally we investigated the viscosity of the L_3 phase in relation with the local structure. The Newtonian behavior observed in DE30UP and DE68 is typical of the L_3 phase, which is due to the fact that the stresses on the membrane are released via rapid reorientation or destruction/creation of the sponge channels.[26] However the stronger temperature dependence of the DDAB/EAN L_3 phase with respect to that of EAN suggests that there is a contribution to the viscosity due to the bicontinuous structure of the L_3 phase. This contribution is quantified via the specific viscosity of the L_3 phase, $\eta_{sp} = \eta/\eta_{EAN} - 1$, where η_{EAN} is the EAN viscosity.

Both η_{sp} and the correlation length (from SANS) are plotted as a function of temperature in Figure S11. Similar temperature dependence is observed for both parameters, which suggest a direct relation between η and ξ. This relation can be explained by the fact that as the correlation length increases, the bilayer is stiffer and hence the viscosity increases. The inset in Figure S11 shows the strong dependence of the viscosity on ξ, given by a power law, $\eta_{sp} \propto \xi^{14}$. The origin of this strong dependence is beyond the scope of the present paper but deserves further study.

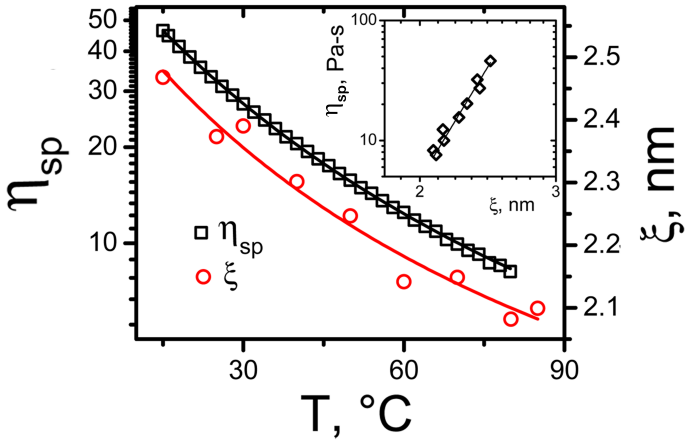

Figure S11. Specific viscosity, η_{sp}, and correlation length, ξ of the DE30UP sample as a function of temperature. The inset shows η_{sp} vs. ξ (Solid line is the fit to the power law $\eta_{sp} \propto \xi^{14}$).

References

(1) Rupert, L. A. M.; Hoekstra, D.; Engberts, J. B. F. N. *J. Am. Chem. Soc.* **1985**, *107*, 2628–2631.

(2) Chen, S. J.; Evans, D. F.; Ninham, B. W. *J. Phys Chem.* **1984**, *88*, 1631–1634.

(3) Barker, J. G.; Glinka, C. J.; Moyer, J. J.; Kim, M. H.; Drews, A. R.; Agamalian, M. *J. App. Cryst.* **2005**, *38*, 1004–1011.

(4) Kline, S. R. *J. App. Cryst.* **2006**, *39*, 895–900.

(5) Underwood, E. E. *Quantitative stereology*; Addison-Wesley: Reading, Mass., 1970.

(6) Dubois, M.; Zemb, T. *Langmuir* **1991**, *7*, 1352–1360.

(7) Teubner, M.; Strey, R. *J. Chem. Phys.* **1987**, *87*, 3195–3200.

(8) Weingärtner, H.; Knocks, A.; Schrader, W.; Kaatze, U. *J. Phys. Chem. A* **2001**, *105*, 8646–8650.

(9) Vogel, H. *Phys. Z.* **1921**, *22*, 645–646.

(10) Tammann, G. *Z. Anorg. Allg. Chem.* **1926**, *156*, 245–247.

(11) Fulcher, G. S. *J. Am. Ceram. Soc.* **1925**, *8*, 339–355.

(12) Vila, J.; Gines, P.; Pico, J. M.; Franjo, C.; Jimenez, E.; Varela, L. M.; Cabeza, O. *Fluid Phase Eq.* **2006**, *242*, 141–146.

(13) Widegren, J. A.; Magee, J. W. *J. Chem. Eng. Data* **2007**, *52*, 2331–2338.

(14) Harris, K. R.; Kanakubo, M.; Woolf, L. A. *J. Chem. Eng. Data* **2007**, *52*, 2425–2430.

(15) Tomida, D.; Kumagai, A.; Kenmochi, S.; Qiao, K.; Yokoyama, C. *J. Chem. Eng. Data* **2007**, *52*, 577–579.

(16) Vila, J.; Varela, L. M.; Cabeza, O. *Electrochim. Acta* **2007**, *52*, 7413–7417.

(17) Restolho, J.; Serro, A. P.; Mata, J. L.; Saramago, B. *J. Chem. Eng. Data* **2009**, *54*, 950–955.

(18) Sescousse, R.; Le, K. A.; Ries, M. E.; Budtova, T. *J. Phys. Chem. B* **2010**, *114*, 7222–7228.

(19) Stoppa, A.; Zech, O.; Kunz, W.; Buchner, R. *J. Chem. Eng. Data* **2010**, *55*, 1768–1773.

(20) Appetecchi, G. B.; Montanino, M.; Carewska, M.; Moreno, M.; Alessandrini, F.; Passerini, S. *Electrochim. Acta* **2011**, *56*, 1300–1307.

(21) Eiden, P.; Bulut, S.; Köchner, T.; Friedrich, C.; Schubert, T.; Krossing, I. *J. Phys. Chem. B* **2011**, *115*, 300–309.

(22) Hiemenz, P. C.; Lodge, T. *Polymer Chemistry*; CRC Press: Boca Raton, FL, 2007.

(23) Duluard, S.; Litas, I.; Bhattacharyya, A. J.; Mauvy, F.; Campet, G.; Delville, M.-H. *Electrochim. Acta* **2010**, *55*, 8839–8846.

(24) Belieres, J.-P.; Angell, C. A. *J. Phys. Chem. B* **2007**, *111*, 4926–4937.

(25) López-Barrón, C. R.; Basavaraj, M. G.; DeRita, L.; Wagner, N. J. *J. Phys. Chem. B* **2012**, *116*, 813–822.

(26) Snabre, P.; Porte, G. *Europhys. Lett.* **1990**, *13*, 641–645.